ETH Library

Controlling the Polarization in Ferroelectric PZT Films via the Epitaxial Growth Conditions

Journal Article

Author(s):
Sarott, Martin F. ; Bucheli, Ursina; Lochmann, Adrian; Fiebig, Manfred ; Trassin, Morgan

Publication date:
2023-07-11

Permanent link:
https://doi.org/https://doi.org/10.3929/ethz-b-000606257

Rights / license:
Creative Commons Attribution 4.0 International

Originally published in:
Advanced Functional Materials 33(28), https://doi.org/10.1002/adfm.202214849

Funding acknowledgement:
- Multifunctional oxide electronics using natural ferroelectric superlattices ()
- Designing oxide electronics with light ()
- Dynamical processes in systems with strong electronic correlations ()

This page was generated automatically upon download from the ETH Zurich Research Collection.
For more information, please consult the Terms of use.

ADVANCED FUNCTIONAL MATERIALS
www.afm-journal.de

Controlling the Polarization in Ferroelectric PZT Films via the Epitaxial Growth Conditions

Martin F. Sarott, Ursina Bucheli, Adrian Lochmann, Manfred Fiebig, and Morgan Trassin**

The integration of thin-film ferroelectrics with reliable properties into oxide electronics requires accomplishing deterministic polarization states. Since ferroelectricity emerges during thin-film synthesis already, it is essential to elucidate how the interplay of different growth parameters affects the polarization. Here, the polarization of fully strained $Pb(Zr_{0.2}Ti_{0.8})O_3$ (PZT) films is accessed in situ, during epitaxial growth. Surprisingly, it is found that the orientation of the out-of-plane polarization during growth may differ from the one after growth completion and it strongly depends on the substrate temperature and the oxygen partial pressure. Increasing the growth temperature and/or the oxygen partial pressure favors a uniform downward-oriented polarization, independent of the direction of polarization during growth. Specifically, for films with an emerging upward-oriented polarization, a polarization reversal and a downward-oriented polarization after cool-down is observed. The in situ measurements obtained by optical second harmonic generation (SHG) in conjunction with ex situ piezoresponse force microscopy (PFM) and X-ray diffraction (XRD) measurements point to the temperature- and pressure-dependent formation of a charged Pb defect gradient toward the film surface as the responsible mechanism for the polarization reorientation.

1. Introduction

Ferroelectric materials are distinguished by a spontaneous and switchable electric polarization. Achieving control over the polarization is essential for their integration into devices, yet it has remained a challenge. Especially in epitaxial thin films, the simultaneous effects of electrostatic, strain, and gradient energies can trigger the formation of complex domain configurations,[1–3] and it becomes increasingly difficult to unravel and act on the microscopic mechanisms that establish the final polarization. Understanding these mechanisms and finally controlling the pristine polarization configuration prior to the application of an external electric field is, however, fundamentally important for a number of applications. For example, the out-of-plane component of the polarization sets the accumulated bound charge at the surface of the ferroelectric, which then regulates the catalytic activity for electrochemical reactions.[4,5] For such applications, post-growth electrical poling on large areas is unfeasible because of the lack of a top electrode. Most importantly, beyond the above mentioned surface-charge control, predetermining the as-grown polarization of thin films removes the need for pre-poling steps in ferroelectric device applications.

Most prototypical ABO_3 perovskite ferroelectrics like $PbTiO_3$, PZT, $BaTiO_3$, and $BiFeO_3$ are already polar at the elevated temperatures during epitaxial thin-film growth[6–8]. Hence, the growth environment of physical vapor deposition processes can strongly affect the polarization of the films. Therefore, when aiming to control the pristine polarization, it is essential to elucidate the individual and the cross-correlated impact of the growth parameters on the polarization. Among the control parameters for epitaxial thin-film synthesis, the following have been identified to influence the polarization of ferroelectric thin films: (i) the surface termination of the substrate, (ii) the oxygen partial pressure, and (iii) the growth temperature.

(i) The choice of buffer layer and its atomic-plane surface termination define the electrostatic screening provided by the bottom interface, and thus set the preferred out-of-plane polarization direction, as has been shown for $BiFeO_3$, $Pb(Zr_xTi_{1-x})O_3$, and $PbTiO_3$.[8–10] (ii) The charge compensation at the film surface depends on the growth atmosphere and can be manipulated by changing the oxygen partial pressure. In ultrathin $PbTiO_3$ films, this has been shown to result in an oxygen-pressure-dependent orientation of the out-of-plane polarization.[11–13] (iii) The temperature-dependent A-site volatility in ferroelectrics like $PbTiO_3$ can be used to tune the formation of charged Pb-vacancy defect complexes.[14] These defect dipoles create an internal field, which can induce the formation of domains and hence allows to control the polarization between a single-domain and a multi-domain configuration simply by adjusting the substrate temperature.

While previous studies have focused on the effects each growth parameter has on its own, their combined influence on the pristine polarization configuration has remained elusive. Such studies are further hampered by difficulties to access

M. F. Sarott, U. Bucheli, A. Lochmann, M. Fiebig, M. Trassin
Department of Materials
ETH Zurich, Vladimir-Prelog-Weg
CH-8093 Zurich, Switzerland
E-mail: martin.sarott@mat.ethz.ch; morgan.trassin@mat.ethz.ch

The ORCID identification number(s) for the author(s) of this article can be found under https://doi.org/10.1002/adfm.202214849.

© 2023 The Authors. Advanced Functional Materials published by Wiley-VCH GmbH. This is an open access article under the terms of the Creative Commons Attribution License, which permits use, distribution and reproduction in any medium, provided the original work is properly cited.

DOI: 10.1002/adfm.202214849

16163028, 2023, 28, Downloaded from https://onlinelibrary.wiley.com/doi/10.1002/adfm.202214849 by Eth Zürich Eth-Bibliothek, Wiley Online Library on [12/07/2023]. See the Terms and Conditions (https://onlinelibrary.wiley.com/terms-and-conditions) on Wiley Online Library for rules of use; OA articles are governed by the applicable Creative Commons License

the dynamics occurring during growth and to disentangle the large number of growth parameters that affect the polarization by changing the electrostatic environment inside the growth chamber.

Here, we track the combined influence of the aforementioned growth parameters during pulsed laser deposition (PLD) on the out-of-plane polarization in epitaxial thin films of the prototypical tetragonal ferroelectric PZT using in situ optical second harmonic generation (ISHG). We complement the in situ experiments by ex situ PFM andXRD measurements, in order to identify the joint contributions of substrate temperature, oxygen partial pressure, and buffer termination to the pristine out-of-plane polarization. We find that the preferred formation of a gradient of positively charged Pb defects with increasing oxygen partial pressure and/or substrate temperature favors a downward-oriented polarization. Hence, the resulting polarization shows a pronounced temperature and pressure dependence, to such an extent that the combined growth parameters can even overrule the bottom interface contribution, which would otherwise enforce an upward-oriented polarization.[8–10] On the contrary, when the buffer termination favors a downward-oriented polarization, we observe robustness of the out-of-plane polarization against growth parameter variations.

Thus, with our work, we provide a recipe to deterministically set the pristine out-of-plane polarization during thin-film synthesis in fully strained, A-site volatile ferroelectric thin films, which is an important milestone for the design of ferroelectric heterostructures and devices.

2. Results and Discussion

We start by tracking the emergence of the ferroelectric polarization during the PLD growth of epitaxial PZT films of 10–15 nm on (110)-oriented $DyScO_3$ (DSO) substrates with a 5 nm conducting $SrRuO_3$ (SRO) buffer layer using ISHG. Optical SHG describes the frequency doubling of light, which is allowed in non-centrosymmetric systems, and thus can be used to probe the inversion-symmetry-breaking spontaneous polarization in ferroelectrics.[15–17] In thin films, the SHG intensity $I_{2\omega}$ relates to the spontaneous polarization P and the film thickness t as, $I_{2\omega} \propto P^2t^2$.[10] In our 45° reflection geometry, we maximize the sensitivity to the out-of-plane polarization by fixing the light polarization of incident and detected SHG light to lie parallel to the plane of reflection.[18] In all our PZT films, the imposed epitaxial strain of –1.41%, considering the high-temperature extrapolated lattice constants of DSO[19] and PZT,[20] increases the ferroelectric Curie temperature.[17,21] This results in growth of PZT in the ferroelectric phase at all growth temperatures investigated in this work (between 550°C and 650°C). To ensure layer-by-layer growth and to measure the film thickness in situ with unit-cell accuracy, we perform reflection high energy electron diffraction (RHEED) simultaneously with the ISHG measurement.

Figure 1a shows the ISHG profiles for the PLD growth of three PZT films at an oxygen partial pressure of 0.05 mbar and at substrate temperatures of 550°C, 600°C, and 650°C. We note that the use of the conducting SRO electrode promotes a single-domain configuration with a preferred upward-oriented polarization due to the SrO self-termination.[8–10,22,23] For all three growth temperatures, a finite ISHG signal above the background level (dashed line) is evident after the deposition of roughly 5–7 nm of PZT (about 3 min deposition time). The steadily increasing ISHG signal with growth time and film thickness is consistent with the appearance of a net out-of-plane ferroelectric polarization. This is supported by room-temperature SHG polarimetry measurements, shown in the inset, where the polarization of the incident light is varied from 0° to 360° at a fixed light polarization of the SHG light of 0° (black, s-polarized) and 90° (red, p-polarized). Our data can be fitted to the *4mm* tetragonal point-group symmetry of PZT with a single-domain out-of-plane polarization. We verified the single-domain, *c*-oriented nature of the films by reciprocal space mapping (not shown). With increasing growth temperature, the ISHG signal during growth evolves qualitatively identically for all films. We only observe a reduction in the ISHG magnitude, resulting from the decrease in spontaneous polarization when approaching the Curie temperature. In striking contrast, the ISHG signal after stopping the PZT deposition shows a strong growth-temperature dependence. At 550°C the ISHG signal remains constant after growth, whereas at 600°C it gets significantly suppressed, and it even drops entirely to the background level for films grown at 650°C. These differences point to a temperature-dependent change in the electrostatic screening of the surface-bound charge, such that increasing the growth temperature tends to destabilize the out-of-plane polarization that is prevalent during growth. Note that the in

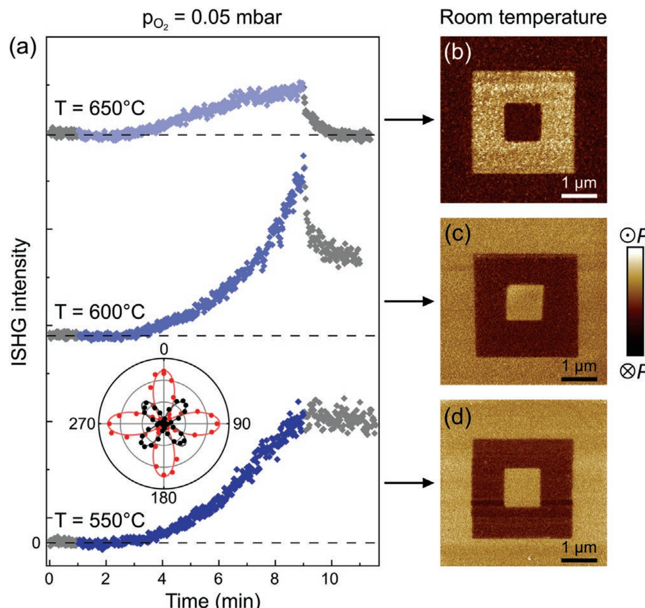

Figure 1. Emergence of the ferroelectric polarization at oxygen partial pressure of 0.05 mbar. a) ISHG signal during the growth of PZT on SRO-buffered DSO at 550°C (bottom), 600°C (middle), and 650°C (top). The grey symbols denote halted growth and the dashed horizontal line represents the paraelectric background level.[18] A vertical offset was added to the ISHG plots for clarity. The inset shows the fitted SHG polarizer measurements after growth at 550°C at a fixed analyzer angle of $\alpha = 0°$ (black) and $\alpha = 90°$ (red). b–d) Out-of-plane PFM images for the films in (a) after reversibly applying a voltage between the scanning tip and the SRO electrode in a box-in-box pattern (∓3*V* for (b) and ±2*V* for (c,d)).

 © 2023 The Authors. Advanced Functional Materials published by Wiley-VCH GmbH

16163028, 2023, 28, Downloaded from https://onlinelibrary.wiley.com/doi/10.1002/adfm.202214849 by Eth Zürich Eth-Bibliothek, Wiley Online Library on [12/07/2023]. See the Terms and Conditions (https://onlinelibrary.wiley.com/terms-and-conditions) on Wiley Online Library for rules of use; OA articles are governed by the applicable Creative Commons License

situ-acquired RHEED patterns stay unchanged when stopping growth, excluding surface reconstruction or laser-beam damage as the cause for the ISHG drop. To visualize the consequences of the changing growth temperature on the ferroelectric domain configuration, we move to ex-situ PFM measurements at room temperature. Figure 1b–d shows the PFM images for the three films after applying box-in-box poling. We find that for the films grown at 550°C (Figure 1d) and 600°C (Figure 1c) the polarization is upward oriented at room temperature, as set by the bottom interface during growth.[9,10,23,24] In contrast, for the highest growth temperature of 650°C, the out-of-plane polarization has changed from the buffer-dictated upward to a downward orientation (Figure 1b). This observation that a change in growth temperature overrules the contribution of the buffer layer is consistent with the report of Weymann et al. on $PbTiO_3$ films grown using radio-frequency magnetron sputtering.[14] Hence, we can deduce that the SHG drop after stopping the PZT growth in Figure 1a corresponds to a destabilization of the upward-oriented polarization in favor of a downward orientation. A polarization reversal with respect to the direction favored by the buffer layer is realized when the growth-stabilized polarization is fully suppressed after growth, as is the case at 650°C. Note that the behavior in Figure 1 is unaffected by variations of the PLD laser fluence.

Next, we investigate the influence of another important PLD growth parameter—the oxygen partial pressure—on the evolution of the polarization during growth. The oxidation conditions of the growth atmosphere have long been recognized as a crucial parameter when growing oxide materials, including ferroelectrics.[12,13,25] In particular, the oxidation state of the deposited species,[26] the stability of the perovskite phase,[27] as well as the concentration of oxygen vacancies have a pronounced effect on the polarization,[28–30] and they all very strongly depend on the oxygen growth pressure.

To elucidate the role of the oxygen partial pressure on the polarization in our PLD-grown films, we consider the ISHG profiles for three PZT films grown at the previous growth temperatures of 550°C, 600°C, and 650°C, but with an increase of the oxygen partial pressure from 0.05 to 0.2 mbar (**Figure 2**a). For this oxygen partial pressure, at 650°C the ISHG signal remains at the background level throughout the entire growth. For the films grown at 550°C and 600°C, we observe a finite ISHG signal during growth consistent with the ferroelectric *4mm* point-group symmetry (fitted SHG polarizer scans in inset) and thus a net out-of-plane polarization. When considering the ISHG evolution after stopping the growth, we find that at 600°C the ISHG signal gets fully suppressed. Only at 550°C the ISHG signal remains at a finite level, showing a striking similarity to the PZT film grown at lower pressure but the higher temperature of 600°C (Figure 1a). Generally, the comparison of the ISHG profiles in Figures 1a and 2a suggest that a pressure increase from 0.05 to 0.2 mbar has the same effect on the polarization as an increase of the growth temperature by 50°C. Hence, for the film deposited at 650°C in the higher oxygen partial pressure, we find ourselves above the Curie temperature during growth with the polarization only emerging during cool-down. This observation strongly suggests a dependence of the Curie temperature in the PZT films on the environment of the growth chamber.

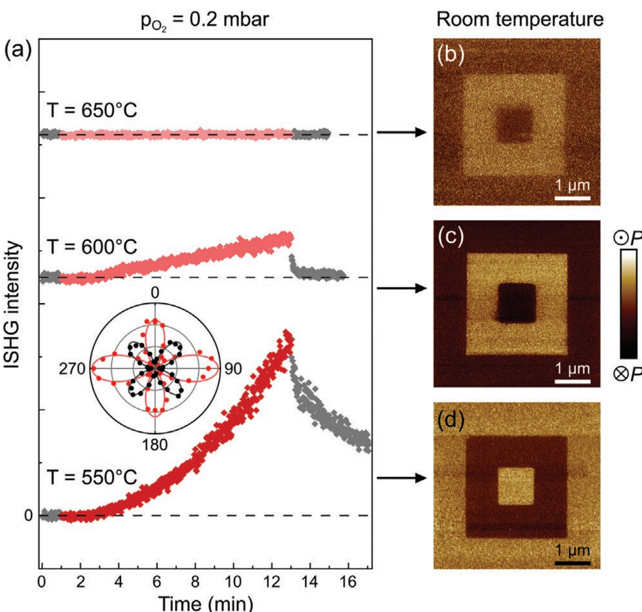

Figure 2. Emergence of the ferroelectric polarization at oxygen partial pressure of 0.2 mbar. a) ISHG signal during the growth of PZT on SRO-buffered DSO at 550°C (bottom), 600°C (middle), and 650°C (top). The grey symbols denote halted growth and the dashed horizontal line represents the paraelectric background level.[18] A vertical offset was added to the ISHG plots for clarity. The inset shows the fitted SHG polarizer measurements after growth at 550°C at a fixed analyzer angle of $\alpha = 0$°C (black) and $\alpha = 90°$ (red). b–d) Out-of-plane PFM images for the films in (a) after reversibly applying a voltage between the scanning tip and the SRO electrode in a box-in-box pattern ($\mp 2V$ for (b,c) and $\pm 2V$ for (d)).

The comparable impact of an increase in growth temperature and an increase in oxygen partial pressure on the polarization is further supported by post-growth PFM measurements shown in Figure 2b–d. Only for films grown at 550°C (Figure 2d) the polarization remains upward oriented, as favored by the SRO buffer layer. At growth temperatures of 600°C or higher (Figure 2b/c), the polarization reverses and is thus entirely downward oriented. We can therefore deduce that an increase in the oxygen partial pressure during growth lowers the transition temperature at which the polarization is preferentially downward oriented.

The pronounced impact of changes in growth temperature and oxygen partial pressure on the emerging polarization that we observe in the ISHG profiles in Figures 1a and 2a indicate a highly susceptible electrostatic environment inside the growth chamber. In particular, we can distinguish two regimes for the evolution of the polarization, as illustrated in **Figure 3**a: (i) During growth, where deposition material is continuously supplied and (ii) after growth, where the film surface settles.

While the growth is in progress, the film polarization is dominated by the termination of the bottom interface favoring an upward orientation.[8,9] The lattice constants and composition of the PZT film are epitaxially stabilized,[31] and the electrostatic screening at the surface is provided by the mobile charged species during the layer-by-layer growth.

After stopping the growth, the surface diffusion of the incoming species stops and the surface settles. This triggers a new electrostatic contribution that can influence the

© 2023 The Authors. Advanced Functional Materials published by Wiley-VCH GmbH

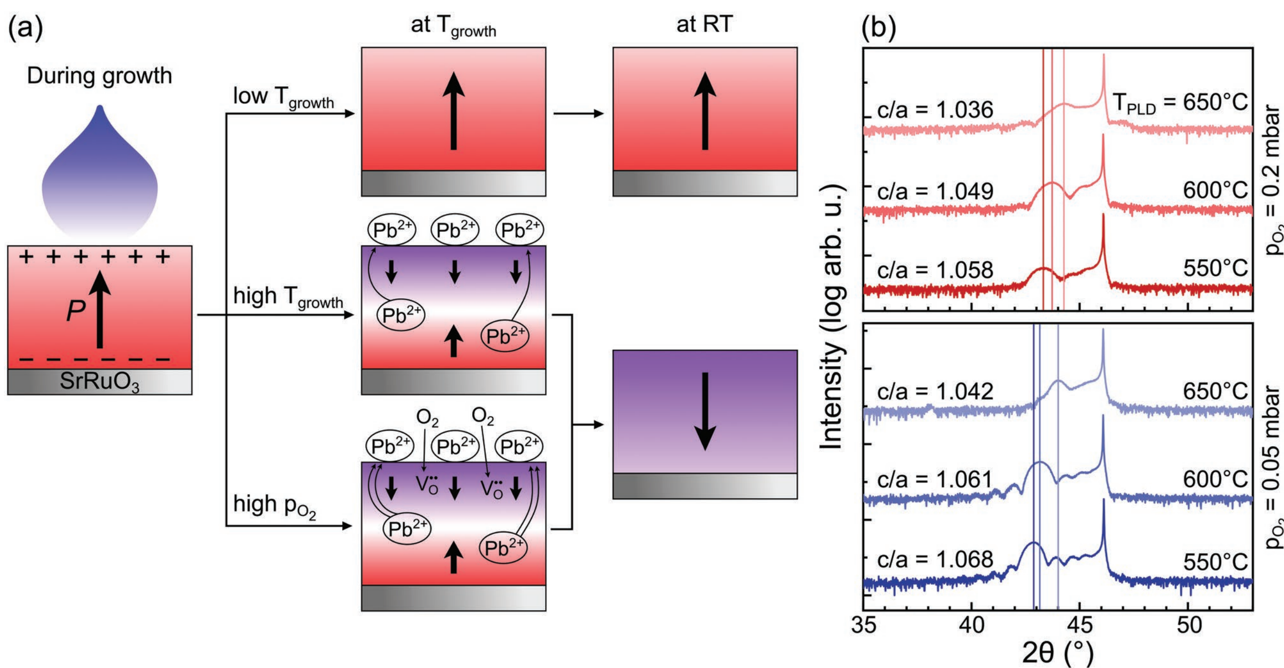

Figure 3. Influence of the varying growth conditions on the polarization of the PZT films. a) Interpretation of the evolution of the polarization in Figures 1 and 2. During growth (left) the bottom interface dominates the polarization direction. After growth at low temperature (top) the growth-stabilized polarization is preserved. High growth temperature (middle) and high oxygen partial pressure (bottom) enhance the accumulation of positively charged Pb defects at the surface, which favor a downward-oriented polarization. b) $\theta-2\theta$ diffractograms around the PZT 002 and DSO 220 peaks with the calculated tetragonality c/a. The vertical lines mark the 2θ position of the PZT 002 peak for all films. A vertical offset was added to the XRD data for clarity.

polarization.[10] In this context, previous studies[10,14] have highlighted the role of the A-site volatility in perovskite ferroelectrics, like PZT and $PbTiO_3$, as well as the influence Pb off-stoichiometries on the polarization. Here, our temperature- and oxygen-pressure-dependent in situ data shed light on how these mechanisms (de)stabilize the polarization inside the growth chamber.

When increasing the growth temperature, for instance, the enhanced volatility and mobility of Pb results in a Pb concentration gradient across the film thickness[14] with an excess of Pb near the newly formed film surface.[10] Note that in addition Pb excess at the surface can also be attributed to the PLD process itself, as light or volatile elements, such as Pb, get enriched in the plasma plume with longer growth duration.[32] As schematically shown in Figure 3a and previously evidenced,[10,14] the positively charged Pb-excess region near the surface, as a result of the Pb concentration gradient, promotes a downward-oriented polarization, opposite to the polarization direction imposed by the buffer layer. This competition reduces the net polarization and causes the ISHG signal to drop upon stopping the growth (Figures 1a and 2a). Here, we have now shown that at sufficiently high temperatures this contribution can entirely suppress the upward-oriented polarization, such that the switched polarization can emerge during cool-down.

In addition, at a fixed growth temperature, the Pb distribution in the films is influenced by the oxygen partial pressure during deposition[12,13,33] (Figure 2). To maintain the neutrality of the system, changes in the concentration of positively charged oxygen vacancies are balanced by varying the amount of positively charged Pb defects present in the films. Hence, as illustrated in Figure 3a, with increasing the oxygen partial pressure during the deposition, the elimination of oxygen vacancies promotes the formation of a stronger gradient consisting of positively charged Pb defects and reduces the transition temperature at which the pristine polarization is fully reversed (see Figure 2). The electrostatic balance between the concentration of oxygen vacancies and Pb defects further stabilizes the Pb gradient and prevents a re-evaporation of Pb in high oxygen partial pressure.

The ISHG profile at our lowest growth temperature of 550°C (Figure 1a), where Pb volatility is less likely to play a role, confirms the dominating influence of the positively charged defects in the post-growth reversal of the polarization. This is reflected in the constant ISHG yield after growth with a persistent upward-oriented polarization, as favored by the bottom interface. Furthermore, on top of the preferred polarization orientation of the Pb defects, we can also recognize a direct influence of the charged defect concentration on the Curie temperature. A similar effect has been previously reported in $BaTiO_3$ films exhibiting defect-dipole ordering.[34] A comparison of the ISHG profiles for the PZT films grown at 650°C in Figures 1a and 2a clearly reveals a suppression of the Curie temperature below 650°C for a higher Pb defect concentration in Figure 2a (zero ISHG signal), whereas it remains above the growth temperature of 650°C in Figure 1a (non-zero ISHG signal).

To investigate how the varying growth conditions affect the average structure and the net polarization in our films, we measure the unit-cell tetragonality c/a using XRD. Based on the strong lattice-polarization coupling in ferroelectrics, the tetragonality has been established to a good approximation[35,36] as an indirect measure of the polarization.[37] Figure 3b shows the $\theta-2\theta$ diffractograms around the PZT 002 and DSO

© 2023 The Authors. Advanced Functional Materials published by Wiley-VCH GmbH

16163028, 2023, 28, Downloaded from https://onlinelibrary.wiley.com/doi/10.1002/adfm.202214849 by Eth Zürich Eth-Bibliothek, Wiley Online Library on [12/07/2023]. See the Terms and Conditions (https://onlinelibrary.wiley.com/terms-and-conditions) on Wiley Online Library for rules of use; OA articles are governed by the applicable Creative Commons License

16163028, 2023, 28, Downloaded from https://onlinelibrary.wiley.com/doi/10.1002/adfm.202214849 by Eth Zürich Eth-Bibliothek, Wiley Online Library on [12/07/2023]. See the Terms and Conditions (https://onlinelibrary.wiley.com/terms-and-conditions) on Wiley Online Library for rules of use; OA articles are governed by the applicable Creative Commons License

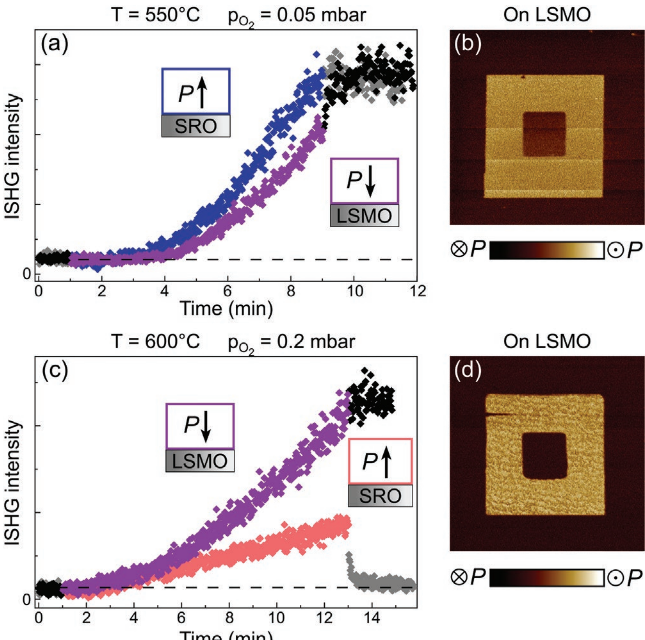

Figure 4. Influence of the buffer termination on the evolution of the polarization. a) ISHG signal for a PZT film grown at low temperature (550°C) and low pressure (0.05 mbar) on LSMO-buffered DSO (purple), in comparison to the PZT film grown under the same conditions on SRO-buffered DSO (blue). The slight ISHG signal enhancement after growth for the downward-polarized film (purple), can be attributed to minor residual Pb accumulation near the surface.[10,23] b) Out-of-plane PFM image for the LSMO-buffered film in (a) at room temperature. c) ISHG signal for a PZT film grown at high temperature (600°C) and low pressure (0.2 mbar) on LSMO-buffered DSO (purple), in comparison to the PZT film grown under the same conditions on SRO-buffered DSO (red). d) Out-of-plane PFM image for the LSMO-buffered film in (c) at room temperature.

220 reflections. When increasing the growth temperature and/or the oxygen partial pressure, we measure a shift of the PZT peak toward higher 2θ values, corresponding to a reduction of the tetragonality c/a in our films. Such a lowered tetragonality indicates a reduced spontaneous polarization,[37] fully consistent with our ISHG data at growth temperature. Remarkably, the observed variation of tetragonality depending on the growth conditions matches with previously reported structural changes associated with Pb off-stoichiometries.[14] This corroborates tuning of the PLD growth parameters as our handle on the polarization.

Having identified the role of temperature and oxygen partial pressure in setting the final polarization in our PZT films, we now turn to the question to what extent the buffer termination determines the post-growth polarization. To clarify this issue, we move to PZT films grown on a MnO_2-terminated $La_{0.7}Sr_{0.3}MnO_3$ (LSMO) buffer layer that now promotes a downward-oriented polarization.[9,10] **Figure 4**a compares the ISHG profiles for the PZT growth on downward-polarization-favoring LSMO and upward-polarization-favoring SRO at 550°C and 0.05 mbar, where, as we have found, the influence of surface Pb off-stoichiometry is small. Indeed, the ISHG signal that depends on the polarization magnitude ($I_{2\omega} \propto P^2$) does not differ much for the two buffer layers during growth despite the opposite polarization direction, as evident from the room-temperature PFM image in Figure 4b.

When we consider the ISHG profiles for the growth on LSMO and SRO at higher temperature and oxygen partial pressure in Figure 4c, where polarization reversal was previously triggered (Figure 2b), we observe a drastically different ISHG behavior for the two buffer layers. On LSMO, which favors a downward-oriented polarization, the ISHG signal is significantly larger than on SRO already during growth, and it remains constant upon stopping the growth. This confirms the previously discussed influence of the Pb defect concentration on the Curie temperature. Here, however, for an emerging polarization with a downward orientation, an increased Pb defect concentration raises the Curie temperature. The ex situ PFM image in Figure 4d further underlines that the downward-oriented polarization, as favored by the LSMO buffer, has not been reversed. Thus, we can infer that an increase of the temperature and/or oxygen partial pressure during the PZT deposition promotes a downward-oriented polarization independent of the polarization preferred by the buffer layer.

3. Conclusion

In summary, we have established a way to control the direction of the out-of-plane polarization in ferroelectric PZT thin films simply by adjusting two central epitaxial PLD growth parameters—substrate temperature and oxygen partial pressure. Their joint effect on the recently identified Pb over-stoichiometry near the film surface[10,14] favors a downward-oriented polarization independently of the electrostatic boundary conditions set by the buffer surface termination. For films with upward-oriented polarization during the growth, this defect-mediated mechanism triggers a full post-growth polarization reversal. The temperature at which the reversal takes place can be adjusted by varying the oxygen partial pressure. In contrast, for films growing downward-polarized, the polarization remains robust against the aforementioned growth parameter changes. Thus, our non-invasive control of the polarization, based on the combined influence of growth temperature and oxygen partial pressure, provides a simple domain-engineering strategy that is of particular use for ferroelectric systems, where conventional electric poling is either inconvenient or impossible.

4. Experimental Section

Thin-Film Growth and Structural Characterization: All thin films in this study were grown using PLD with a KrF excimer laser (248 nm) on (110)-oriented DSO substrates (CrysTec GmbH). The SRO buffer layers were grown at 700°C with an oxygen partial pressure of 0.015 mbar at a laser fluence of 0.95 Jcm^{-2} at 2Hz. For the LSMO buffer layers, prior to LSMO deposition, a single unit cell of TiO_2 was grown (to ensure MnO_2 termination) at 700°C with an oxygen partial pressure of 0.015 mbar at a laser fluence of 0.95 Jcm^{-2} at 2 Hz. The LSMO was subsequently deposited at the same growth conditions, but at 1 Hz. PZT layers were grown at three different temperatures (550°C, 600°C, 650°C) and two different oxygen partial pressures (0.05 mbar, 0.2 mbar) with a laser fluence of 1.2 Jcm^{-2} at 4 Hz. For all films grown at an oxygen partial pressure of 0.05 mbar or lower, the thickness was monitored in situ using RHEED. Layer thicknesses were confirmed ex situ via X-ray reflectivity.

Surface-topography and PFM experiments were performed on a Bruker Multimode 8 atomic force microscope with Pt-coated Si tips from MikroMasch ($k = 5.4$ Nm^{-1}). For PFM, we used $V_{ac} = 0.75$ V at 10 kHz.

© 2023 The Authors. Advanced Functional Materials published by Wiley-VCH GmbH

In Situ Optical Second Harmonic Generation: Light pulses at a wavelength of 800 nm with a pulse duration of 45 fs and a repetition rate of 1 kHz were generated by an amplified Ti:Sapphire laser system and subsequently converted into the fundamental light with $\lambda = 1200$ nm by an optical parametric amplifier. The pulse energy was set to 20 µJ and the incident light was focused onto the thin films in the vacuum chamber under an incidence angle of 45° with a spot diameter of 250 µm. The generated SHG signal at 600 nm was detected by a photomultiplier system after passing through a monochromator. For all ISHG measurements, the polarization of the incident fundamental light and of the frequency-doubled light was set to be parallel to the plane of reflection.

SHG Polarimetry Analysis: Optical SHG was described by the equation $P_i(2\omega) = \varepsilon_0 \chi^{(2)}_{ijk} E_j(\omega) E_k(\omega)$ with $P_i(2\omega)$ and $E_{j,k}(\omega)$ being the electric-field components of the SHG and the fundamental light, respectively. The non-zero components of the rank-three tensor $\chi^{(2)}_{ijk}$ are determined by the crystallographic point group of the system under study. In case of *4mm* point-group symmetry of PZT with an out-of-plane polarization (*z*), the following $\chi^{(2)}_{ijk}$ tensor components are permitted to be non-zero: $\chi^{(2)}_{zzz}$, $\chi^{(2)}_{zyy} = \chi^{(2)}_{zxx}$, $\chi^{(2)}_{yzy} = \chi^{(2)}_{xzx} = \chi^{(2)}_{yyz} = \chi^{(2)}_{xxz}$. Using these components and following the procedure described in [15], we can fit the SHG polarizer measurements.

Acknowledgements

M.F.S. and M.T. acknowledge the Swiss National Science Foundation Spark funding CRSK-2_196061. M.T. acknowledges the financial support by the Swiss National Science Foundation under project no. 200021_188414. M.F. acknowledges financial support by the Swiss National Science Foundation under project no. 200021_178825.

Open access funding provided by Eidgenossische Technische Hochschule Zurich.

Conflict of Interest

The authors declare no conflict of interest.

Author Contributions

M.F.S. and M.T. designed the experiment. M.F.S. supported by U.B. and A.L. grew the thin films. M.F.S. conducted the ISHG measurements, SHG polarimetry analysis, PFM measurements, and XRD characterization. M.F.S., M.T., and M.F. wrote the manuscript with input from all authors. M.T. supervised the work jointly with M.F. All authors discussed the results and contributed to the completion of the manuscript.

Data Availability Statement

The data that support the findings of this study are available from the corresponding author upon reasonable request.

Keywords

charged point defects, epitaxy, ferroelectrics, nonlinear optics, PZT, thin films

Received: December 20, 2022
Revised: March 15, 2023
Published online: March 31, 2023

[1] Y. L. Tang, Y. L. Zhu, X. L. Ma, A. Y. Borisevich, A. N. Morozovska, E. A. Eliseev, W. Y. Wang, Y. J. Wang, Y. B. Xu, Z. D. Zhang, S. J. Pennycook, *Science* **2015**, *348*, 547.
[2] S.-L. Hsu, M. R. McCarter, C. Dai, Z. Hong, L.-Q. Chen, C. T. Nelson, L. W. Martin, R. Ramesh, *Adv. Mater.* **2019**, *31*, 1901014.
[3] Y. J. Wang, Y. P. Feng, Y. L. Zhu, Y. L. Tang, L. X. Yang, M. J. Zou, W. R. Geng, M. J. Han, x. W. Guo, B. Wu, X. L. Ma, *Nat. Mater.* **2020**, *19*, 881.
[4] A. Kakekhani, S. Ismail-Beigi, *ACS Catal.* **2015**, *5*, 4537.
[5] I. Efe, N. A. Spaldin, C. Gattinoni, *J. Chem. Phys.* **2021**, *154*, 024702.
[6] K. J. Choi, M. Biegalski, Y. L. Li, A. Sharan, J. Schubert, R. Uecker, P. Reiche, Y. B. Chen, X. Q. Pan, V. Gopalan, L.-Q. Chen, D. G. Schlom, C. B. Eom, *Science* **2004**, *306*, 1005.
[7] N. A. Pertsev, A. G. Zembilgotov, A. K. Tagantsev, *Phys. Rev. Lett.* **1998**, *80*, 1988.
[8] G. De Luca, N. Strkalj, S. Manz, C. Bouillet, M. Fiebig, M. Trassin, *Nat. Commun.* **2017**, *8*, 1419.
[9] P. Yu, W. Luo, D. Yi, J. X. Zhang, M. D. Rossell, C.-H. Yang, L. You, G. Singh-Bhalla, S. Y. Yang, Q. He, Q. M. Ramasse, R. Erni, L. W. Martin, Y. H. Chu, S. T. Pantelides, S. J. Pennycook, R. Ramesh, *PNAS* **2012**, *109*, 9710.
[10] N. Strkalj, C. Gattinoni, A. Vogel, M. Campanini, R. Haerdi, A. Rossi, M. D. Rossell, N. A. Spaldin, M. Fiebig, M. Trassin, *Nat. Commun.* **2020**, *11*, 5815.
[11] R. V. Wang, D. D. Fong, F. Jiang, M. J. Highland, P. H. Fuoss, C. Thompson, A. M. Kolpak, J. A. Eastman, S. K. Streiffer, A. M. Rappe, G. B. Stephenson, *Phys. Rev. Lett.* **2009**, *102*, 047601.
[12] M. J. Highland, T. T. Fister, D. D. Fong, P. H. Fuoss, C. Thompson, J. A. Eastman, S. K. Streiffer, G. B. Stephenson, *Phys. Rev. Lett.* **2011**, *107*, 187602.
[13] G. B. Stephenson, M. J. Highland, *Phys. Rev. B.* **2011**, *84*, 064107.
[14] C. Weymann, C. Lichtensteiger, S. Fernandez-Pena, A. B. Naden, L. R. Dedon, L. W. Martin, J.-M. Triscone, P. Paruch, *Adv. Electron. Mater.* **2020**, *6*, 2000852.
[15] S. A. Denev, T. T. A. Lummen, E. Barnes, A. Kumar, V. Gopalan, *J. Am. Cerm. Soc.* **2011**, *94*, 2699.
[16] J. Kaneshiro, Y. Uesu, T. Fukui, *J. Opt. Soc. Am. B* **2010**, *27*, 888.
[17] M. F. Sarott, E. Gradauskaite, J. Nordlander, N. Strkalj, M. Trassin, *J. Phys.: Condens. Matter* **2021**, *33*, 293001.
[18] M. F. Sarott, M. D. Rossell, M. Fiebig, M. Trassin, *Nat. Commun.* **2022**, *13*, 3159.
[19] M. D. Biegalski, J. H. Haeni, S. Trolier-McKinstry, D. G. Schlom, C. D. Brandle, A. J. Ven Graitis, *J. Mater. Res.* **2005**, *20*, 952.
[20] Y. Kuroiwa, Y. Terado, S. J. Kim, A. Sawada, Y. Yamamura, S. Aoyagi, E. Nishibori, M. Sakata, M. Takata, *Jpn. J. Appl. Phys.* **2005**, *44*, 7151.
[21] N. A. Pertsev, V. G. Kukhar, H. Kohlstedt, R. Waser, *Phys. Rev. B* **2003**, *67*, 054107.
[22] H. G. Lee, L. Wang, L. Si, X. He, D. G. Porter, J. R. Kim, E. K. Ko, J. Kim, S. M. Park, B. Kim, A. T. S. Wee, A. Bombardi, Z. Zhong, T. W. Noh, *Adv. Mater.* **2020**, *32*, 1905815.
[23] C. Gattinoni, N. Strkalj, R. Haerdi, M. Fiebig, M. Trassin, N. A. Spaldin, *PNAS* **2020**, *117*, 28589.
[24] M. F. Sarott, M. Fiebig, M. Trassin, *Appl. Phys. Lett.* **2020**, *117*, 132901.
[25] F. Gunkel, D. V. Christensen, Y. Z. Chen, N. Pryds, *Appl. Phys. Lett.* **2020**, *116*, 120505.
[26] R. Groenen, J. Smit, K. Orsel, A. Vailionis, B. Bastiaens, M. Huijben, K. Boller, G. Rijnder, G. Koster, *APL Mater.* **2015**, *3*, 070701.
[27] G. R. Fox, S. B. Krupanidhi, *J. Mater. Res.* **1994**, *9*, 699.
[28] P. Nukala, M. Ahmadi, Y. Wei, S. De Graaf, E. Stylianidis, T. Chakrabortty, S. Matzen, H. W. Zandbergen, A. Björling, D. Mannix, D. Carbone, B. Kooi, B. Noheda, *Science* **2021**, *6542*, 630.
[29] J. F. Scott, M. Dawber, *Appl. Phys. Lett.* **2000**, *76*, 3801.

© 2023 The Authors. Advanced Functional Materials published by Wiley-VCH GmbH

16163028, 2023, 28, Downloaded from https://onlinelibrary.wiley.com/doi/10.1002/adfm.202214849 by Eth Zürich Eth-Bibliothek, Wiley Online Library on [12/07/2023]. See the Terms and Conditions (https://onlinelibrary.wiley.com/terms-and-conditions) on Wiley Online Library for rules of use; OA articles are governed by the applicable Creative Commons License

[30] W. Peng, J. Mun, Q. Xie, J. Chen, L. Wang, M. Kim, T. W. Noh, *npj Quantum Mater.* **2021**, *6*, 48.
[31] O. Y. Gorbenko, X. V. Samoilenkov, I. E. Graboy, A. R. Kaul, *Chem. Mater.* **2002**, *14*, 4026.
[32] C. W. Schneider, T. Lippert, *Appl. Phys. A* **2023**, *129*, 138.
[33] A. N. Morozovska, E. A. Eliseev, N. V. Morozovsky, S. V. Kalinin, *Phys. Rev. B* **2017**, *95*, 195413.
[34] A. R. Damodaran, E. Breckenfeld, Z. Chen, S. Lee, L. W. Martin, *Adv. Mater.* **2014**, *26*, 6341.
[35] T. Grande, J. R. Tolchard, S. M. Selbach, *Chem. Mater.* **2012**, *24*, 338.
[36] U. Aschauer, R. Pfenninger, S. M. Selbach, T. Grande, N. A. Spaldin, *Phys. Rev. B* **2013**, *88*, 054111.
[37] C. Lichtensteiger, J.-M. Triscone, J. Junquera, P. Ghosez, *Phys. Rev. Lett.* **2005**, *94*, 047603.

© 2023 The Authors. Advanced Functional Materials published by Wiley-VCH GmbH

16163028, 2023, 28, Downloaded from https://onlinelibrary.wiley.com/doi/10.1002/adfm.202214849 by Eth Zürich Eth-Bibliothek, Wiley Online Library on [12/07/2023]. See the Terms and Conditions (https://onlinelibrary.wiley.com/terms-and-conditions) on Wiley Online Library for rules of use; OA articles are governed by the applicable Creative Commons License